

Effects of irradiation on superconducting properties of small-grained MgB_2 thin films

Li Liu(刘丽), Jung Min Lee, Yoonseok Han, Jaegu Song, Chorong Kim, Jaekwon Suk, Won Nam Kang, Jie Liu(刘杰), Soon-Gil Jung, and Tuson Park

Citation: Chin. Phys. B, 2023, 32 (**12**): 127402. DOI: 10.1088/1674-1056/acf5d3
Journal homepage: http://cpb.iphy.ac.cn; http://iopscience.iop.org/cpb

What follows is a list of articles you may be interested in

Role of grain boundary networks in vortex motion in superconducting films

Yu Liu(刘宇), Feng Xue(薛峰), and Xiao-Fan Gou(苟晓凡)
Chin. Phys. B, 2023, 32 (**12**): 127401. DOI: 10.1088/1674-1056/ace315

Barrier or easy-flow channel: The role of grain boundary acting on vortex motion in type-II superconductors

Yu Liu(刘宇), Xiao-Fan Gou(苟晓凡), and Feng Xue(薛峰)
Chin. Phys. B, 2021, 30 (**9**): 097402. DOI: 10.1088/1674-1056/ac11ea

Effect of graphene grain boundaries on MoS_2/graphene heterostructures

Yue Zhang(张悦), Xiangzhe Zhang(张祥喆), Chuyun Deng(邓楚芸), Qi Ge(葛奇), Junjie Huang(黄俊杰), Jie Lu(卢捷), Gaoxiang Lin(林高翔), Zekai Weng(翁泽锴), Xueao Zhang(张学骜), Weiwei Cai(蔡伟伟)
Chin. Phys. B, 2020, 29 (**6**): 067403. DOI: 10.1088/1674-1056/ab8a37

Optimization of intergrain connection in high-temperature superconductor $Bi_2Sr_2CaCu_2O_x$

Li Cheng-Shan (李成山), Zhang Sheng-Nan (张胜楠), Hao Qing-Bin (郝清滨), Ma Xiao-Bo (马小波), Lu Tian-Ni (卢天倪), Zhang Ping-Xiang (张平祥)
Chin. Phys. B, 2015, 24 (**7**): 077401. DOI: 10.1088/1674-1056/24/7/077401

Fabrication and properties of high performance $YBa_2Cu_3O_{7-\delta}$ radio frequency SQUIDs with step-edge Josephson junctions

Liu Zheng-Hao (刘政豪), Wei Yu-Ke (魏玉科), Wang Da (王达), Zhang Chen (张琛), Ma Ping (马平), Wang Yue (王越)
Chin. Phys. B, 2014, 23 (**9**): 097401. DOI: 10.1088/1674-1056/23/9/097401

Effects of irradiation on superconducting properties of small-grained MgB_2 thin films

Li Liu(刘丽)[1,2,3,4], Jung Min Lee[2], Yoonseok Han[2], Jaegu Song[2], Chorong Kim[5], Jaekwon Suk[5], Won Nam Kang[2,†], Jie Liu(刘杰)[3,4,‡], Soon-Gil Jung[6,§], and Tuson Park[1,2,¶]

[1] *Center for Quantum Materials and Superconductivity (CQMS), Sungkyunkwan University, Suwon* 16419, *Republic of Korea*
[2] *Department of Physics, Sungkyunkwan University, Suwon* 16419, *Republic of Korea*
[3] *Institute of Modern Physics, Chinese Academy of Sciences (CAS), Lanzhou* 730000, *China*
[4] *School of Nuclear Science and Technology, University of Chinese Academy of Sciences (UCAS), Beijing* 100049, *China*
[5] *Korea Multi-purpose Accelerator Complex, Korea Atomic Energy Research Institute, Gyeongju, Gyeongbuk* 38180, *Republic of Korea*
[6] *Department of Physics Education, Sunchon National University, Suncheon* 57922, *Republic of Korea*

(Received 20 June 2023; revised manuscript received 21 August 2023; accepted manuscript online 1 September 2023)

We investigate the effect of ion irradiation on MgB_2 thin films with small grains of approximately 122 nm and 140 nm. The flux pinning by grain boundaries is insignificant in the pristine MgB_2 films due to good inter-grain connectivity, but is significantly improved after 120-keV Mn–ion irradiation. The scaling behavior of the flux pinning force density for the ion-irradiated MgB_2 thin films with nanoscale grains demonstrates the predominance of pinning by grain boundaries, in contrast to the single-crystalline MgB_2 films where normal point pinning was dominant after low-energy ion irradiation. These results suggest that irradiation-induced defects can accumulate near the grain boundaries in metallic MgB_2 superconductors.

Keywords: MgB_2 films, grain boundaries, flux pinning, low-energy ion irradiation

PACS: 74.70.Ad, 74.25.Wx, 61.72.Mm, 61.80.Lj **DOI:** 10.1088/1674-1056/acf5d3

1. Introduction

MgB_2 has tremendous potential for practical applications owing to its excellent superconducting properties. For instance, the superconducting critical temperature (T_c) of MgB_2 is approximately 40 K, which makes it a promising material for use in liquid-helium-free apparatus.[1] Its high upper critical field (H_{c2}) makes MgB_2 a suitable alternative for commercial superconductors in high-field magnet applications.[2–4] Moreover, from the aspect of radioactivity, MgB_2 is one of the promising materials in neutron irradiation environment, such as fusion reactor, because of its shorter half-life of the induced activity than Nb-based superconducting alloys.[5] Grain boundaries (GBs) in MgB_2 function as a strong pinning site owing to its large coherence length (ξ). In addition, no weak link behavior across GBs is observed in MgB_2, which is in contrast to the weak link behavior in high-T_c cuprate superconductors.[6] Therefore, a kilometer-long MgB_2 superconducting wire used in real systems can be fabricated using a simple powder-in-tube technique, thus considerably reducing the manufacturing cost.[7,8]

The high current-carrying capability for superconductors necessary for practical applications in magnetic field environment can be achieved by introducing artificial defects.[9] Particle irradiation is a suitable method for producing defects in superconducting materials and has been successfully used in roll-to-roll 80-m long $YBa_2Cu_3O_{7-\delta}$ coated conductors.[10,11] The effect of irradiation on MgB_2 has been widely studied since it discovered in 2001.[12] Neutron has been suggested as a potential irradiating source for MgB_2 due to the large thermal neutron capture cross section of the ^{10}B atom ($\sim 20\%$ in natural B), which causes defects through the $^{10}B(n, \alpha)^7Li$ reaction.[13] The self-shielding effect of the ^{10}B atoms induces inhomogeneous defects around the surface. However, homogeneous damage can be achieved by replacing ^{10}B with ^{11}B isotope.[14,15]

The GBs in metals are known to act as an effective sink for irradiation-induced defects.[16] Irradiation-induced defects, such as vacancies and interstitials, including injected ions can easily migrate into the GBs because the defect diffusion barrier near GBs is considerably lower than the defect diffusion barrier within the grains.[17,18] Moreover, the process of absorbing irradiation-induced defect clusters around GBs has also been observed by *in situ* transmission electron microscope.[19,20] Hence, the radiation tolerance of nanocrystalline materials is larger than that of coarse-grained samples, which can be improved as the density of GBs increases.[21,22]

Considering the metallic characteristics of MgB_2 superconductors,[23] it can be assumed that ion irradiation has

†Corresponding author. E-mail: wnkang@skku.edu
‡Corresponding author. E-mail: j.liu@impcas.ac.cn
§Corresponding author. E-mail: sgjung@scnu.ac.kr
¶Corresponding author. E-mail: tp8701@skku.edu

© 2023 Chinese Physical Society and IOP Publishing Ltd

a significant influence on grain boundary pinning of MgB_2 with small grain sizes. In this study, we irradiated 120-keV Mn ions on MgB_2 thin films with nanoscale grain sizes. The critical current density (J_c) of the pristine MgB_2 samples was rapidly decreased with the increase in magnetic field owing to a good inter-grain connectivity. However, the field performance of J_c of the irradiated films was significantly improved with the change of the flux pinning mechanism from weak to strong pinning. The scaling behavior of the flux pinning is consistent with the dominance of surface pinning in the irradiated films, underpinning that GBs in MgB_2 can act as an effective sink of irradiation-induced defects.

2. Material and methods

The *c*-axis-oriented MgB_2 thin films with grain sizes of approximately 122 nm and 140 nm were fabricated using a hybrid physical-chemical vapor deposition (HPCVD) system, and the details of the fabrication condition and quality of films were described everywhere.[24–26] The *c*-cut Al_2O_3 substrate of 10 mm×10 mm in size was placed on the susceptor filled with 99.99% purity Mg pieces. The carrier gas was H_2 at a flow rate of 80 sccm, and the susceptor was heated to 700 °C in a total pressure of 100 Torr (1 Torr = 1.33322×10^2 Pa). Subsequently, 5% B_2H_6 in H_2 gas (20 sccm) was introduced into the chamber to grow the MgB_2 thin films. The growth rate of the films was approximately 2.5 nm/s.

Ion irradiation was performed at the Korea Multi-purpose Accelerator Complex (KOMAC). The prepared MgB_2 films were cut into several pieces for irradiation at each fluence, and each MgB_2 film with thicknesses of 250 nm (MB250) and 430 nm (MB430) were irradiated at room temperature using Mn ions with a beam energy of 120 keV and fluences of 1×10^{13} (1E13), 5×10^{13} (5E13), and 1×10^{14} (1E14) ions/cm^2. The direction of the incident ions was tilted by 7° from the *c* axis to minimize the channeling effect. The damage events produced in the MgB_2 thin films by 120-keV Mn ions were determined using the Monte Carlo simulation program, the stopping and range of ions in matter (SRIM).[27]

The crystal phases and orientations of the prepared films were checked by x-ray diffraction (XRD), and average grain sizes of the films were evaluated by counting the number of grains in the area through the surface morphology observed by scanning electron microscopy (SEM). The zero-field-cooled (ZFC) and field-cooled (FC) dc magnetization (M) as well as magnetization hysteresis (M–B) loops were measured by using magnetic property measurement system (MPMS, Quantum Design) equipped with a 5-T superconducting magnet. The direction of the magnetic field was parallel to the *c*-axis direction of the film. The J_c value was calculated from the M–B loops using the Bean critical-state model $J_c = 15\Delta M/r$, where ΔM is the width of the M–B loops per volume (in units of emu/cm^3) and r is the radius corresponding to the total area (S) of the film surface, *i.e.*, $S = \pi r^2$.[28,29]

3. Results and discussion

The displacements per atom (dpa) produced in the MgB_2 by 120-keV Mn–ion irradiation with fluences of 1E13, 5E13, and 1E14 ions/cm^2 was simulated using the transport of ions in matter (TRIM) code in the SRIM software,[27,30] as shown in Fig. 1. The inset in Fig. 1 is a schematic diagram of the MgB_2 thin film with a thickness of 250 nm (MB250) after 120-keV Mn–ion irradiation, divided into two regions, namely irradiated and unirradiated regions. The thickness of the irradiated region (t_D) was determined at the dpa = 0.001 because this value has an impact on the field performance of J_c of MgB_2,[31] and the t_D for 1E13, 5E13, and 1E14 Mn ions/cm^2 were approximately 136 nm, 160 nm, and 170 nm, as indicated by the arrows in Fig. 1.

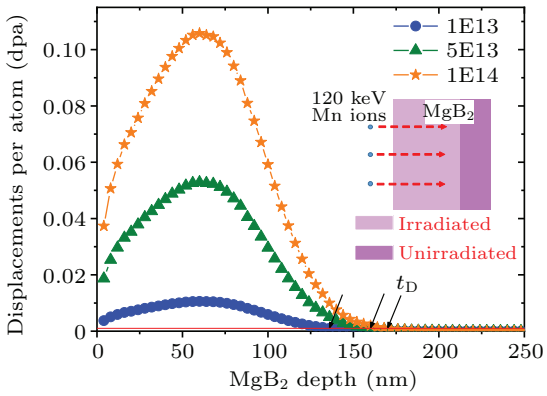


Fig. 1. Displacements per atom (dpa) as a function of MgB_2 depth, generated by 120-keV Mn–ion irradiation with fluences of 1E13, 5E13, and 1E14 ions/cm^2. Inset illustrates the schematic view of irradiated and unirradiated areas in 250-nm-thick MgB_2 thin film, where the depth of irradiated region (t_D) is determined at 0.001 dpa, as indicated by the red solid line and arrows.

Figure 2(a) shows XRD pattern of θ–2θ scan for pristine MB250 (MB250-PRI) deposited on *c*-cut Al_2O_3 substrate, indicating a highly *c*-axis orientation. Figure 2(b) is the surface morphology of MB250 observed by SEM. The estimated average grain diameter of MB250 was approximately 122 nm. The magnetic field dependence of critical current density (J_c) of MB250-PRI at 5 K and 20 K is illustrated in Fig. 2(c). A large self-field $J_c \approx 19$ MA/cm^2 at 20 K and its rapid reduction in magnetic field indicate the high quality of the fabricated films.[32] The self-field J_c is lower at 5 K than at 20 K due to a large flux jump at low fields, as shown in inset of Fig. 2(c), which is known as a result of thermomagnetic instability.[33] The flux pinning force density (F_p) as a function of the magnetic field presented in Fig. 2(d) reflects the high quality of MB250. Here, F_p was calculated using the relation $F_p = J_c \times B$. The sharp peak of $F_p(B)$ curves at low fields is thought to be caused by the rapid decrease in $J_c(B)$ due to the lack of effective pinning sites.[34]

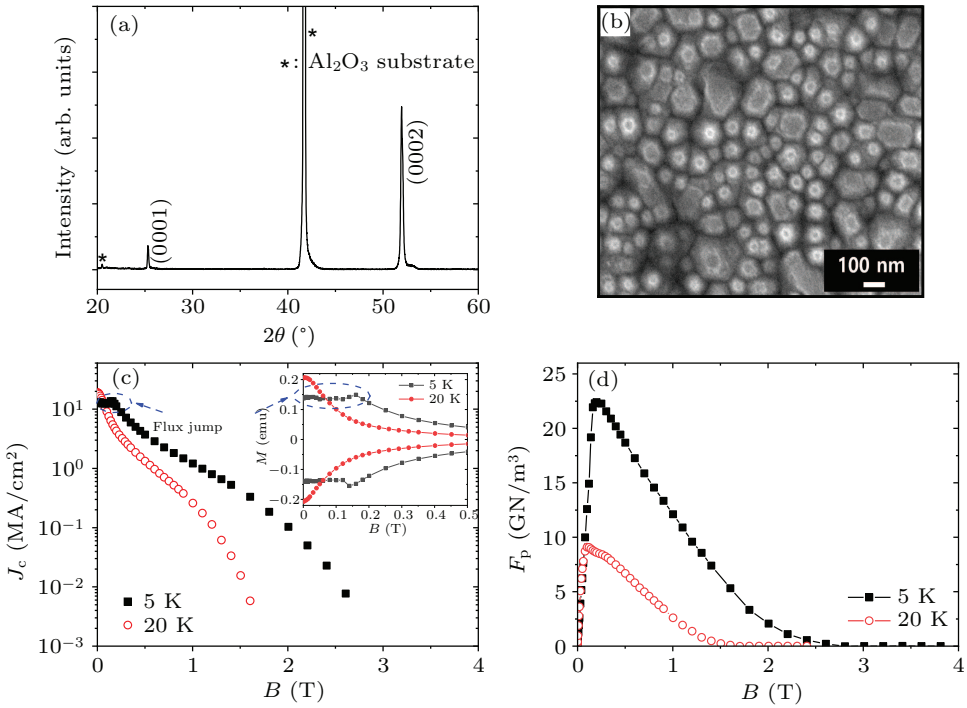


Fig. 2. (a) XRD pattern of a θ–2θ scan for MB250-PRI deposited on a c-cut Al_2O_3 substrate. (b) SEM surface morphology of MB250-PRI where the average grain diameter is approximately 122 nm. (c) Semi-logarithmic J_c–B curves at 5 K and 20 K for MB250-PRI. Inset shows the M–B hysteresis curves at 5 K and 20 K, indicating a presence of large flux jump at 5 K. (d) Magnetic field dependence of volume flux pinning force density (F_p) at 5 K and 20 K for MB250-PRI.

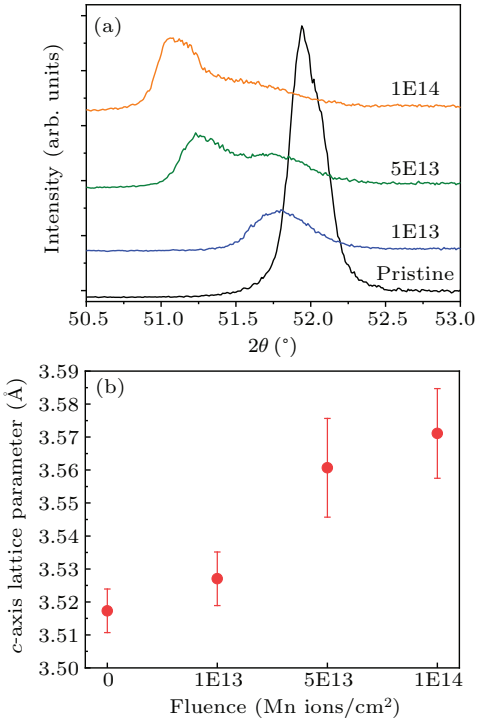


Fig. 3. (a) Enlarged view of (0002) peak of MB250 before and after 120-keV Mn–ion irradiation. For the sample irradiated with a fluence of 5×10^{13} ions/cm^2, the small broad peak near (0002) peak was related to the remaining unirradiated layer. (b) Changes in c-axis lattice constant of MB250 films as a function of ion fluence.

The changes in c-axis lattice parameter before and after irradiation was characterized by XRD. After irradiation, the (000l) peaks of MB250 shift toward lower angle. For the sake of clarity, an enlarged view of (0002) peak is shown in Fig. 3(a). The existence of a broad peak in the sample irradiated at a fluence of 5×10^{13} ions/cm^2 is due to the unirradiated layer, as shown in schematic diagram of Fig. 1. The c-axis parameter calculated from (0002) peak of MB250 increases monotonically with increasing ion fluence, as shown in Fig. 3(b), reaching the increment of about 1.53% compared to the pristine sample at a maximum fluence of 1×10^{14} ions/cm^2.

The superconducting transition temperature (T_c) of MB250 was gradually decreased by increasing the amount of irradiated Mn ions. Figure 4 shows the zero-field-cooled (ZFC) and field-cooled (FC) dc magnetization (M) at 5 Oe as a function of temperature for MB250 before and after 120-keV Mn-ion irradiation with fluences of 1E13, 5E13, and 1E14 ions/cm^2. The MB250-PRI shows a T_c of 38.7 K (corresponding to the transition of 10% in ZFC $M(T)$ curve) with a sharp transition width $\Delta T_c = 1.8$ K determined using the transition of 90% to 10% of the superconducting diamagnetic signal in the ZFC $M(T)$ curve, as presented in Fig. 4. The T_c gradually decreased whereas ΔT_c increased as the fluence level increases, and at the highest fluence level of 1E14 ions/cm^2, T_c and ΔT_c were 28.2 K and 6.9 K, respectively.

The reduction of T_c by low-energy ion irradiations can be understood due to the formation of point defects and lattice distortions in MgB_2.[35,36] The irradiation-induced disorder can act as impurity scattering centers, thus enhancing inter-band scattering and suppressing T_c.[15,37,38] In addition, a decrease in the electron–phonon coupling constant with increasing dpa leads to a suppression of T_c.[39,40]

The magnetic field dependence of J_c at 5 K and 20 K for

MB250 before and after 120-keV Mn–ion irradiation is shown in Figs. 5(a) and 5(b), respectively. The J_c at low fields is decreased gradually with increasing fluence, associated with a suppression of T_c, and at both temperatures, the magnitude of the self-field J_c was suppressed by approximately a factor of 10 at the highest fluence of 1E14 Mn ions/cm^2. However, the field performance of J_c was significantly improved after irradiation. For MB250 irradiated with 1E13 Mn ions/cm^2, the J_c value increased more than 10-fold from approximately 0.02 for the pristine sample to 0.26 MA/cm^2 at 5 K and 2.4 T. Figures 5(c) and 5(d) plot the flux pinning force density (F_p) as a function of the magnetic field, calculated from the $J_c(B)$ curves in Figs. 5(a) and 5(b), respectively. For the sample irradiated with 1E13 Mn ions/cm^2, F_p at 5 K and 20 K obviously increased at high fields larger than $B > 1$ T, indicating that the number of effective pinning sites for high fields was increased by irradiation. The significantly decreased F_p at low fields was caused by the decrease in J_c with the suppression of T_c after irradiation.

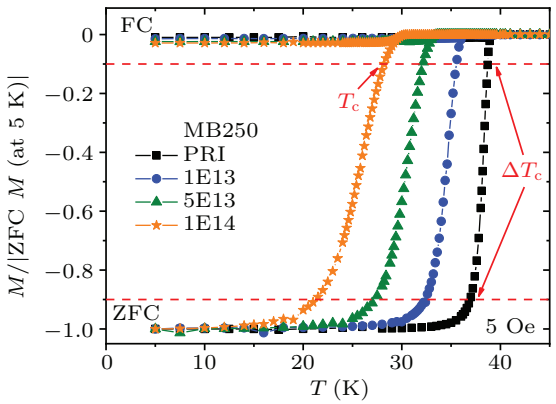


Fig. 4. Temperature dependence of ZFC and FC M at 5 Oe for pristine (PRI) and 120-keV Mn–ion irradiated MB250, where the $M(T)$ values were normalized by the absolute ZFC M value at 5 K for comparisons. Superconducting transition width (ΔT_c) was defined as the difference between the 10% and 90% transitions of the diamagnetic signal from the normal state and denoted by the arrows with a red color.

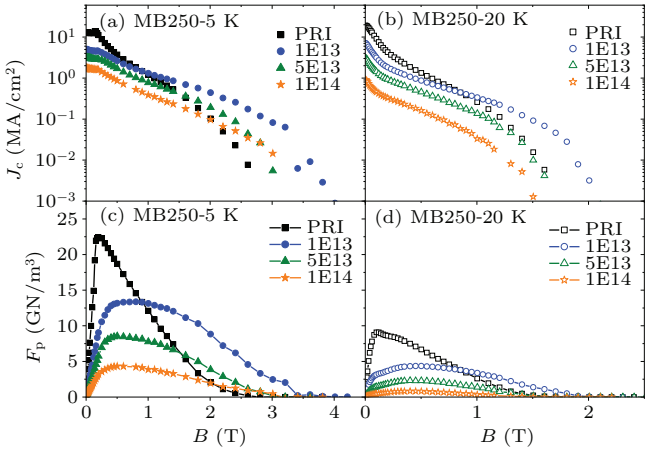


Fig. 5. Semi-logarithmic J_c–B curves at (a) 5 K and (b) 20 K for MB250 before and after irradiation. The field performance of J_c is improved by Mn ion irradiation, while the J_c at low fields decreases gradually as the fluence level increases. Magnetic field dependence of F_p is plotted at (c) 5 K and (d) 20 K.

The scaling behavior of the normalized flux pinning force density ($f_p = F_p/F_{p,max}$) with respect to the reduced magnetic field ($b = B/B_{irr}$) for irradiated MB250 was studied, where $F_{p,max}$ is the maximum F_p and B_{irr} is the irreversible magnetic field. Since the J_c and F_p values of type-II superconductors approach zero when the magnetic field is equal to B_{irr}, if the B_{irr} value is not close to B_{c2}, B_{irr} is more suitable for describing the b value to investigate the scaling behavior of flux pinning force.[41,42] The B_{irr} value of the pristine and irradiated MB250 was estimated using the Kramer plot of $J_c^{0.5}B^{0.25} \propto (B_{irr} - B)$,[43,44] as described in Figs. 6(a) and 6(b). Figures 6(c) and 6(d) show the f_p *versus* b curve for MB250 at 5 K and 20 K, respectively.

In the scaling law of flux pinning force, $f_p(b) \propto b^p(1-b)^q$, the peak position of $f_p(b)$ together with parameters p and q is dependent on the characteristics of the dominant pinning source of superconducting samples.[44–46] According to Dew–Hughes (DH) model, the $f_p(b)$ peak is located at $b = 0.2$ ($p = 0.5$ and $q = 2$) for surface pinning and $b = 0.33$ ($p = 1$ and $q = 2$) for normal point pinning, as shown in Fig. 6(c).[46] The $f_p(b)$ curves for MB250-PRI cannot be explained by any pinning models, to the best of our knowledge, because of the low density of effective pinning centers, as discussed in Fig. 2(d). However, the flux pinning mechanism of the irradiated MB250 samples showed the predominance of surface pinning. In contrast, since low-energy ion irradiation primarily produces homogeneously distributed point defects caused by nuclear stopping of energetic ions, as depicted in the inset of Fig. 6(d),[47] in general, single-crystalline MgB_2 films showed the dominance of normal point pinning after low-energy ion irradiation.[48,49]

The effect of GBs on the irradiation-induced defects in the relatively thicker MgB_2 films with a thickness of 430 nm (MB430) was additionally studied in comparison with the thickness of the irradiated regions. The XRD results of the MB430 are shown in Fig. 7(a). The (0002) peak clearly splitting into two peaks for the fluence level $> 1 \times 10^{13}$ ions/cm^2 due to the presence of thicker unirradiated layer compared to MB250. The c-axis lattice parameter corresponding to the 2nd peak (irradiated layer) increases with increasing fluence, whereas that of the 1st peak (unirradiated layer) in MB430 is hardly changed, as shown in Fig. 7(b). Figures 7(c) and 7(d) show the magnetic field dependence of J_c for MB430 at 5 K and 20 K, respectively, and the inset in Fig. 7(d) is a top SEM view of MB430, indicating small grains with an average size of approximately 140 nm. The improvement in the field performance of J_c for the irradiated MB430 showed similar feature to that in case of the irradiated MB250, whereas the decrease in J_c at low fields was comparatively small. The small decrease in low-field J_c for irradiated MB430 can be thought to be due to the giant proximity effect between the irradiated and unirradiated layers.[50,51]

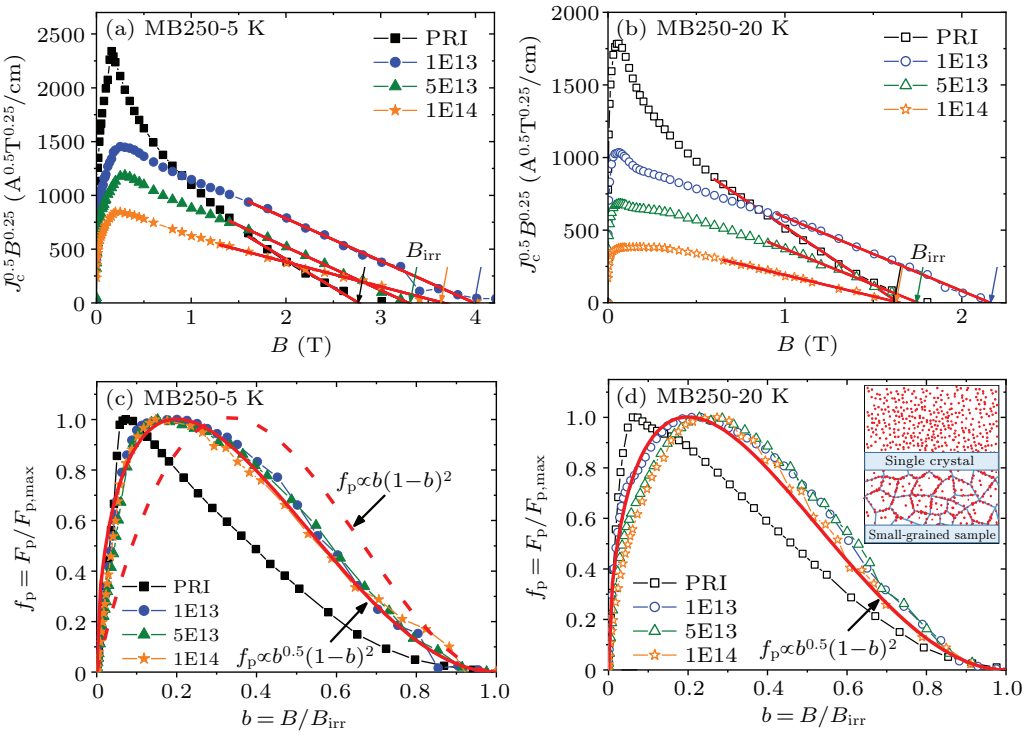


Fig. 6. Kramer plots for pristine and 120-keV Mn–ion-irradiated MB250 at (a) 5 K and (b) 20 K to evaluate irreversible field (B_{irr}) indicated by arrows. Normalized flux pinning force density (f_p) with respect to reduced magnetic field (b) at (c) 5 K and (d) 20 K for pristine and 120-keV Mn-ion-irradiated MB250. The red solid line and the red dashed line represent the fitting curves for surface pinning and normal point pinning, respectively. Inset of Fig. 5(d) illustrates the schematic view of the distribution of irradiation-induced defects in single crystals and the films with small grains.

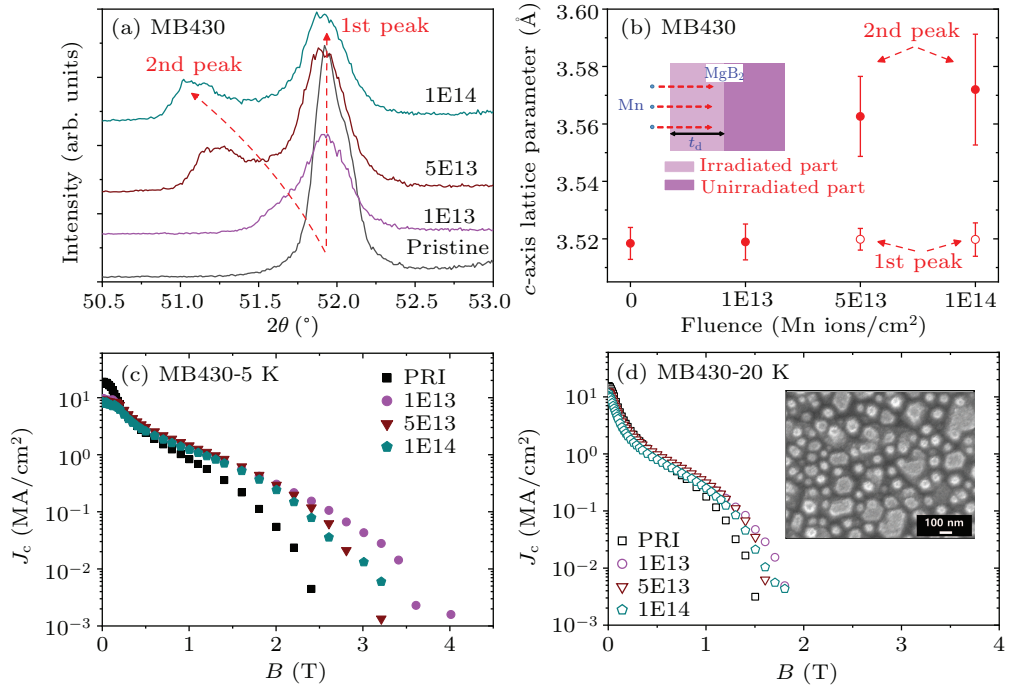


Fig. 7. (a) XRD patterns of MB430 around the (0002) peak of MgB_2. (b) Variation of c-axis lattice constant of MB430 with fluence. (c)–(d) Magnetic field dependence of critical current density (J_c) at (c) 5 K and (d) 20 K for 430-nm-thick MgB_2 films (MB430) before and after 120-keV Mn–ion irradiation. The inset in (d) is the top SEM view for MB430 with an average grain diameter of approximately 140 nm.

The Kramer plots for MB430 at 5 K and 20 K are shown in Figs. 8(a) and 8(b), respectively, and the B_{irr} for each sample was indicated by arrows. Figures 8(c) and 8(d) show normalized flux pinning force as a function of the reduced magnetic field for MB430 at 5 K and 20 K, respectively. The $f_p(b)$ at high fields for $b > 0.2$ and at 5 K overlapped accurately with surface pinning. Although the $f_p(b)$ curve exhibits a slight deviation at 20 K, the flux pinning by GBs is still effective even when the thickness of MgB_2 films is relatively larger than that of the irradiated layer t_D. These results further support the improvement of the flux pinning effect by GBs in MgB_2 thin films after irradiation. The sharp peak in the $f_p(b)$ curve at low fields was almost suppressed

in the irradiated MB250, as shown in Fig. 6, indicating that the residual sharp peak of $f_p(b)$ at low fields in the irradiated MB430 is associated with the unirradiated region. Our findings can provide useful information for designing radiation resistant MgB_2 because grain boundaries in metallic MgB_2 superconductors can be acted as an effective sink of irradiation-induced defects, thus irradiation tolerance of MgB_2 can be enhanced by decreasing grain size.

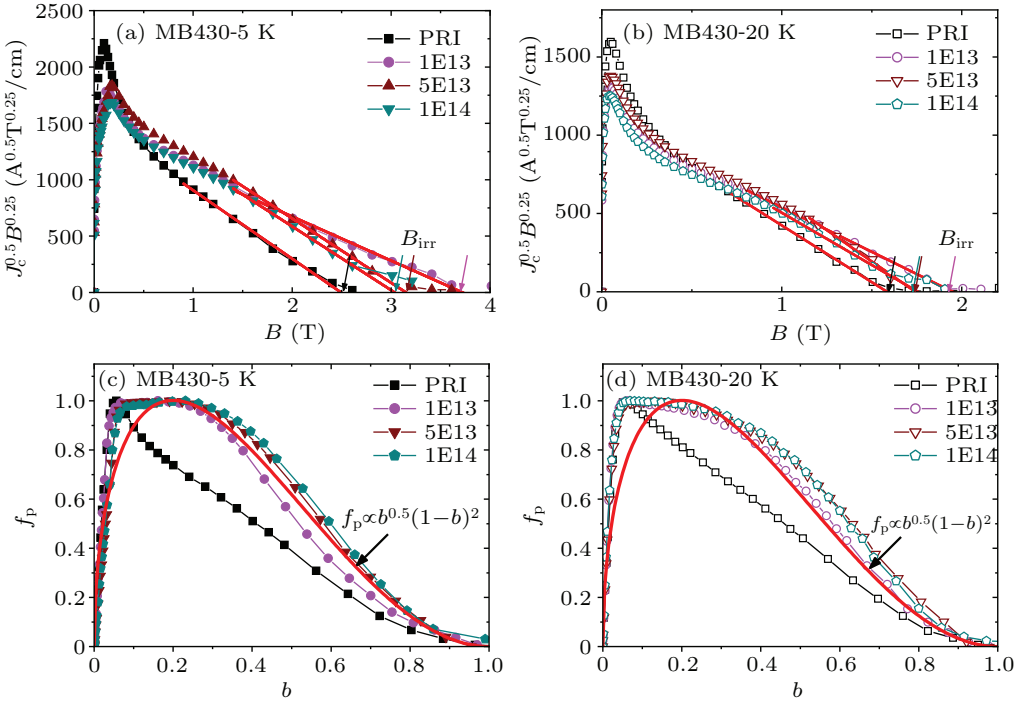


Fig. 8. Kramer plots for pristine and 120-keV Mn–ion-irradiated MB430 at (a) 5 K and (b) 20 K. Here, B_{irr} is indicated by arrows. Scaling behavior of the flux pinning force for MB430 at (c) 5 K and (d) 20 K indicates that the effect of surface pinning is enhanced significantly after ion irradiation.

4. Conclusions

In summary, we observed that the pinning effect by GBs in MgB_2 thin films can be improved by ion irradiation. The MgB_2 thin films with nanoscale grains of approximately 122 nm and 140 nm were irradiated with 120-keV Mn ions leading to a significant increase in the field performance of J_c for all films as compared with that of J_c for pristine films. Although the GBs of pristine films were not effective for flux pinning, the scaling behavior of the flux pinning force showed that the surface pinning, *i.e.*, grain boundary pinning, became dominant after ion irradiation. These findings underpin that MgB_2 superconductors with small grains can be a good candidate for application in irradiation environments, such as nuclear fusion reactor.

Acknowledgements

We wish to acknowledge the support of the accelerator group and operators of KOMAC (KAERI (C. K., J. S.)). Project supported by the National Research Foundation (NRF) of Korea through a grant funded by the Korean Ministry of Science and ICT (Grant No. 2021R1A2C2010925 (T. P., Y. H., J. S.)); the Basic Science Research Program through the NRF of Korea funded by the Ministry of Education (Grant Nos. NRF-2019R1F1A1055284 (J. M. L., W. N. K.) and NRF-2021R1I1A1A01043885 (S. G. J., Y. H.)), the National Natural Science Foundation of China (Grant Nos. 12035019 (J. L.)). Moreover, L. L. would like to acknowledge the Chinese Scholarship Council (CSC) for fellowship support.

References

[1] Ye S J, Song M, Matsumoto A, Togano K, Takeguchi M, Ohmura T and Kumakura H 2013 *Supercond. Sci. Technol.* **26** 125003
[2] Vinod K, Kumar R G A and Syamaprasad U 2007 *Supercond. Sci. Technol.* **20** R1
[3] Ferrando V, Orgiani P, Pogrebnyakov A V, Chen J, Li Q, Redwing J M, Xi X X, Giencke J E, Eom C B, Feng Q R, Betts J B and Mielke C H 2005 *Appl. Phys. Lett.* **87** 252509
[4] Jun B H, Kim J H, Kim C J and Choo K N 2015 *J. Alloys Compd.* **650** 794
[5] Noda T, Takeuchi T and Fujita M 2004 *J. Nucl. Mater.* **329** 1590
[6] Mikheenko P, Martínez E, Bevan A, Abell J S and MacManus-Driscoll J L 2007 *Supercond. Sci. Technol.* **20** S264
[7] Tanaka H, Suzuki T, Kodama M, Koga T, Watanabe H, Yamamoto A and Michizono S 2020 *IEEE Trans. Appl. Supercond.* **30** 6200105
[8] Yang Y, Sumption M D, Rindfleisch M, Tomsic M and Collings E W 2021 *Supercond. Sci. Technol.* **34** 025010
[9] Larbalestier D, Gurevich A, Feldmann D M and Polyanskii A 2001 *Nature* **414** 368
[10] Kwok W K, Welp U, Glatz A, Koshelev A E, Kihlstrom K J and Crabtree G W 2016 *Rep. Prog. Phys.* **79** 116501
[11] Rupich M W, Sathyamurthy S, Fleshler S, Li Q, Solovyov V, Ozaki T, Welp U, Kwok W K, Leroux M, Koshelev A E, Miller D J, Kihlstrom K, Civale L, Eley S and Kayani A 2016 *IEEE Trans. Appl. Supercond.* **26** 6601904

[12] Nagamatsu J, Nakagawa N, Muranaka T, Zenitani Y and Akimitsu J 2001 *Nature* **410** 63
[13] Eisterer M, Zehetmayer M, Tönies S, Weber H W, Kambara M, Babu N H, Cardwell D A and Greenwood L R 2002 *Supercond. Sci. Technol.* **15** L9
[14] Putti M, Braccini V, Ferdeghini C, Gatti F, Grasso G, Manfrinetti P, Marré D, Palenzona A, Pallecchi I, Tarantini C, Sheikin I, Aebersold H U and Lehmann E 2005 *Appl. Phys. Lett.* **86** 112503
[15] Putti M, Affronte M, Ferdeghini C, Manfrinetti P, Tarantini C and Lehmann E 2006 *Phys. Rev. Lett.* **96** 077003
[16] Singh B N 1974 *Philos. Mag.* **29** 25
[17] Liu L L, Tang Z, Xiao W and Wang Z 2013 *Mater. Lett.* **109** 221
[18] Arjhangmehr A and Feghhi S A H 2016 *Sci. Rep.* **6** 23333
[19] Sun C, Song M, Yu K Y, Chen Y, Kirk M, Li M, Wang H and Zhang X 2013 *Metall. Mater. Trans. A* **44** 1966
[20] El-Atwani O, Hinks J A, Greaves G, Gonderman S, Qiu T, Efe M and Allain J P 2014 *Sci. Rep.* **4** 4716
[21] Bai X M and Uberuaga B P 2013 *Jom* **65** 360
[22] Xiao X Z, Chu H J and Duan H L 2016 *Sci. China-Phys. Mech. Astron.* **59** 664601
[23] Bud'Ko S L, Petrovic C, Lapertot G, Cunningham C E, Canfield P C, Jung M H and Lacerda A H 2001 *Phys. Rev. B* **63** 220503
[24] Seong W K, Oh S J and Kang W N 2012 *Jpn. J. Appl. Phys.* **51** 083101
[25] Seong W K 2009 *Growth mechanism and superconductivity in MgB_2 nano-structures and single-crystalline MgB_2 thin film*, Ph.D. dissertation (Suwon: Sungkyunkwan University) (in Korea)
[26] Seong W K, Huh J Y, Kang W N, Kim J W, Kwon Y S, Yang N K and Park J G 2007 *Chem. Vap. Deposition* **13** 680
[27] Ziegler J F 2004 *Nucl. Instrum. Method Phys. Res. B* **219–220** 1027
[28] Bean C P 1964 *Rev. Mod. Phys.* **36** 31
[29] Kim H J, Kang W N, Choi E M, Kim M S, Kim K H P and Lee S I 2001 *Phys. Rev. Lett.* **87** 087002
[30] Egeland G W, Valdez J A, Maloy S A, McClellan K J, Sickafus K E and Bond G M 2013 *J. Nucl. Mater.* **435** 77
[31] Bugoslavsky Y, Cohen L F, Perkins G K, Polichetti M, Tate T J, Gwilliam R and Caplin A D 2001 *Nature* **411** 561
[32] De-Silva K S B, Aboutalebi S H, Xu X, Wang X L, Li W X, Konstantinov K and Dou S X 2013 *Scr. Mater.* **69** 437
[33] Choi E M, Lee H S, Kim H J, Lee S I, Kim H J and Kang W N 2004 *Appl. Phys. Lett.* **84** 82
[34] Koblischka M R, Wiederhold A, Koblischka-Veneva A, Chang C, Berger K, Nouailhetas Q, Douine B and Murakami M 2020 *AIP Adv.* **10** 015035
[35] Le T, Pham H H, Nghia N T, Nam N H, Miyanaga T, Tran D H and Kang W N 2023 *Ceram. Int.* **49** 2715
[36] Kar'kin A E, Voronin V I, D'yachkova T V, Kadyrova N I, Tyutyunik A P, Zubkov V G, Zanulin Y G, Sadovski M V and Goshchitski B N 2001 *JETP Lett.* **73** 570
[37] Wang Y, Bouquet F, Sheikin I, Toulemonde P, Revaz B, Eisterer M, Weber H W, Hinderer J and Junod A 2003 *J. Phys.: Condens. Matter* **15** 883
[38] Erwin S C and Mazin I I 2003 *Phys. Rev. B* **68** 132505
[39] Lee J M, Jung S G, Han Y, Park T H, Jang J, Jeon H, Yeo S, Choi H Y, Park T and Kang W N 2022 *Supercond. Sci. Technol.* **35** 015001
[40] Pham H H, Le T, Nguyen T N, Nam N H, Nguyen N T, Sohn M K, Kang D J, Park T, Yun J, Lee Y, Kim J, Tran D H and Kang W N 2023 *Ceram. Int.* **49** 20586
[41] Martínez E, Mikheenko P, Martínez-López M, Millán A, Bevan A and Abell J S 2007 *Phys. Rev. B* **75** 134515
[42] Takahashi K, Kitaguchi H and Doi T 2009 *Supercond. Sci. Technol.* **22** 025008
[43] Keys S A and Hampshire D P 2003 *Supercond. Sci. Technol.* **16** 1097
[44] Kramer E J 1973 *J. Appl. Phys.* **44** 1360
[45] Koblischka M R and Murakami M 2000 *Supercond. Sci. Technol.* **13** 738
[46] Dew-Hughes D 1974 *Philos. Mag.* **30** 293
[47] Bowden P and Brandon D G 1963 *J. Nucl. Mater.* **9** 348
[48] Pham D, Jung S G, Tran D H, Park T and Kang W N 2019 *J. Appl. Phys.* **125** 023904
[49] Jung S G, Son S K, Pham D, Kang W N, Lim W C, Song J and Park T 2019 *J. Phys. Soc. Jpn.* **88** 034716
[50] Jung S G, Pham D, Park T H, Choi H Y, Seo J W, Kang W N and Park T 2019 *Sci. Rep.* **9** 3315
[51] Jung S G, Pham D, Lee J M, Han Y, Kang W N and Park T 2021 *Curr. Appl. Phys.* **22** 14